Supporting Information

Synthesis and Molecular Sieving Mechanism of Millet-derived Carbon Molecular Sieves for Separation of C4 Olefins

Jiaying Wang [a], Zhijie Wen [b], Qibin Xia [b], Lisa Mingzhe Sun [c], Junliang Wu [a], Xin Zhou [b*], Zhong Li [b*]*

[a] *School of Environment and Energy, South China University of Technology, Guangzhou, PR China*

[b] *School of Chemistry and Chemical Engineering, South China University of Technology, Guangzhou, PR China*

[c] *School of Chemical Engineering, University of Birmingham, Birmingham, B15 2TT, UK*

List of contents

Section 1 Figures

- Figure S1. Breakthrough experiment setup
- Figure S2. TG-DTG curves of millet
- Figure S3. Kinetic curves of C_4H_6 adsorption in the samples
- Figure S4. Cycling breakthrough performance of MCMS-700 and MCMS-800
- Figure S5. Mechanical strength of the samples

Section 2 Tables

- Table S1. Relevant physical properties of C4 olefins and paraffins
- Table S2. Porosity parameters of the samples
- Table S3. The pore structure parameters of the samples
- Table S4. sp^2-C/sp^3-C ratios of the samples
- Table S5. Element compositions of the samples from XPS

Section 1 Figures

Figure S1 Self-assembly breakthrough experiment setup

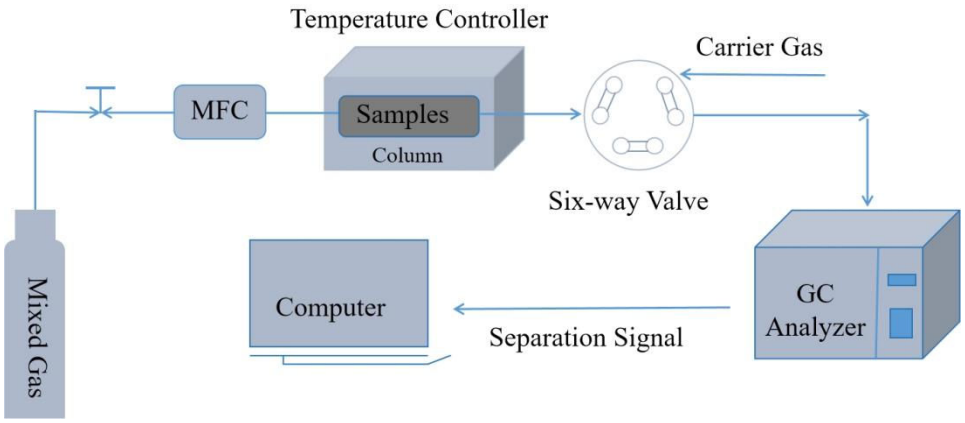

Fig. S1 Self-assembly breakthrough experiment setup

Figure S2 TG-DTG curves of millet

Fig. S2 presents the thermogravimetric-differential thermogravimetric (TG-DTG) curves of millet, illustrating its thermal degradation behavior during pyrolysis. The initial mass loss observed around 140 °C is attributed to the evaporation of adsorbed moisture and bound water. As the temperature increased to approximately 300 °C, a more pronounced mass loss event occurred, primarily resulting from the decomposition of labile oxygen-containing functional groups on the millet surface. Above 350 °C, the sample continued to lose mass, but the mass loss rate diminished gradually. This phenomenon indicates the sustained pyrolysis of residual oxygen-containing functional groups, whose abundance decreased with the progression of the reaction.

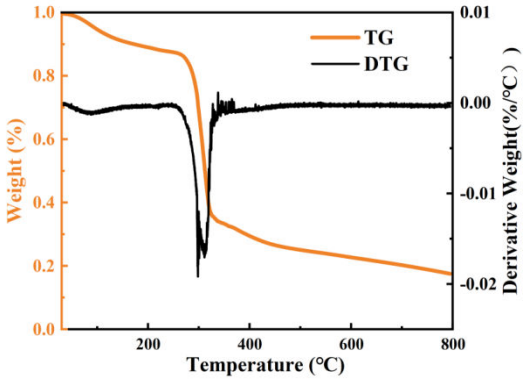

Fig. S2 TG-DTG curves of millet

Figure S3 Kinetic curves of C_4H_6 adsorption in the samples

Adsorption kinetics is an important parameter for evaluating the mass transfer rate of adsorbates in adsorbents, which is essential for designing the adsorption separation processes. **Fig. S3** demonstrates the adsorption kinetic curves of C4 olefins on MCMSs (at 298 K and 0.5 bar). It can be seen that the adsorption rate of C_4H_6 on MCMS-800 is faster than that on MCMS-700 since the former has a somewhat larger pore size than the latter.

According to the kinetic curves, the diffusion coefficient D for C_4H_6 was calculated using the micropore diffusion model described below.[1-4]

$$\frac{q_t}{q_e} \approx \frac{6}{\sqrt{\pi}}\sqrt{\frac{Dt}{r^2}} \qquad (\frac{q_t}{q_e} < 0.3)$$

Where t is the adsorption time (min); q_t is the instantaneous adsorption capacity at time t (mmol/g); q_e is the equilibrium adsorption capacity (mmol/g); D is the intraparticle diffusion coefficient (cm^2/min or cm^2/s); and r is the average radius of the adsorbent particles (cm).

As shown in **Fig. S3(c-d),** plotting q_t/q_e against $\sqrt{t}$ yields straight lines in the initial uptake region, with slopes proportional to $\sqrt{\frac{D}{r^2}}$. Accordingly, the values of D/r^2 of C_4H_6 on MCMS-700 and MCMS-800 can be obtained.

Owing to the irregular morphology of the MCMS particles, their actual radius r cannot be precisely determined. Therefore, we define $D' = D/r^2$ (min^{-1}) as the apparent diffusion coefficient to evaluate the adsorption kinetic behavior of C_4H_6 within MCMS.

The apparent diffusion coefficients D' of C_4H_6 on MCMS-700 and MCMS-800 samples are calculated to be 6.23×10^{-4} min^{-1} and 1.13×10^{-3} min^{-1}, respectively.

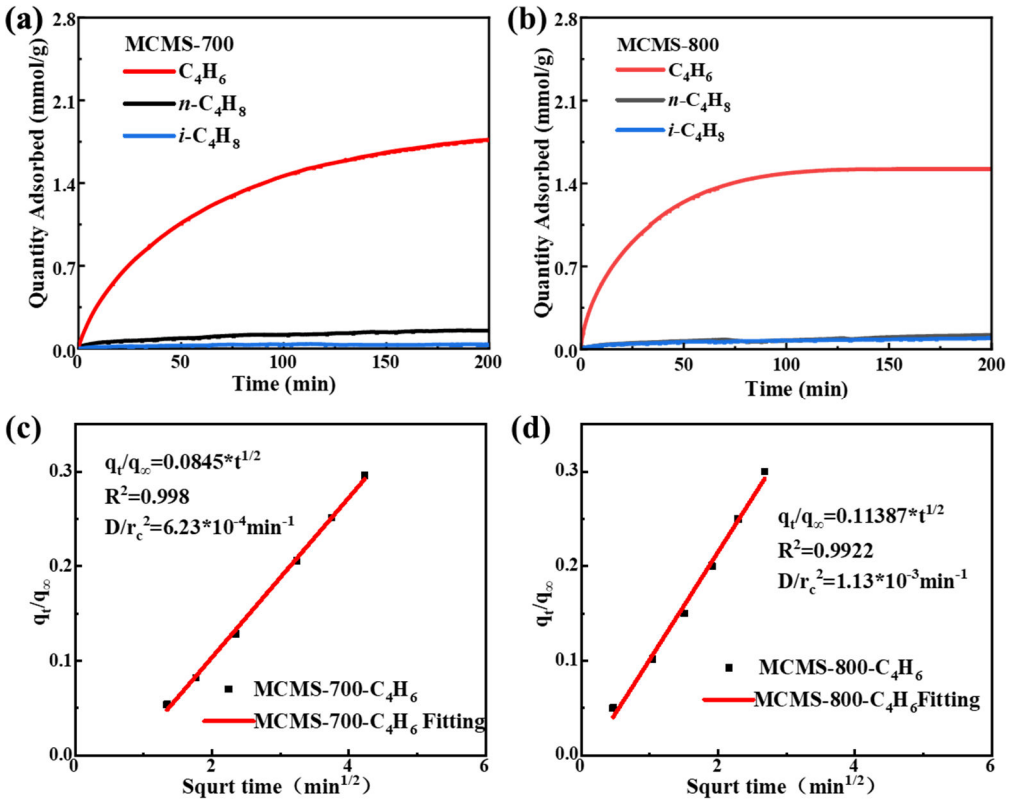

Fig. S3 Adsorption kinetics of C_4H_6 on the samples

Figure S4 Cycling breakthrough performance of MCMS-700 and MCMS-800

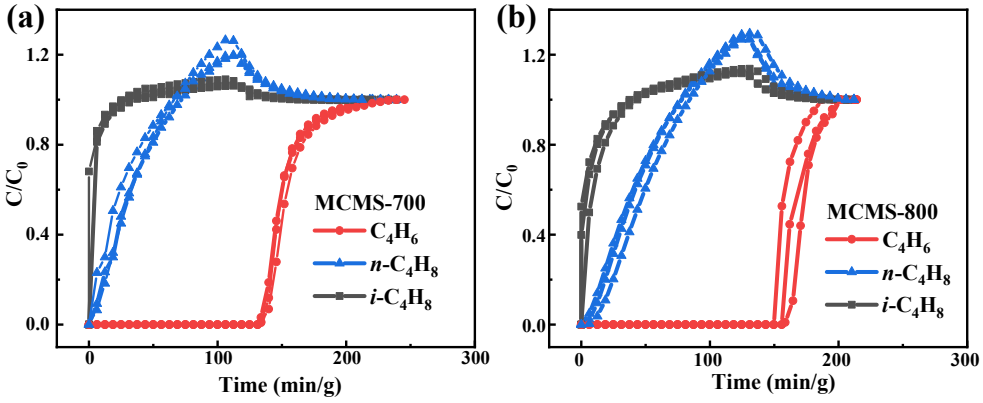

Fig. S4 Three consecutive breakthrough cycles of the C_4H_6/*i*-C_4H_8/*n*-C_4H_8 ternary mixture over the fixed beds of (a) MCMS-700 and (b) MCMS-800 at 298 K

Figure S5 Mechanical strength of the samples

Fig.S5 shows the mechanical strength of the resultant samples. When loading such MCMS particles into a fixed bed, the following precautions should be noted: layered support screens shall be installed during the packing of granular adsorbents. This

measure is primarily intended to disperse the gravity load of the upper-layer adsorbents and prevent the bottom adsorbents from crushing and pulverization under excessive pressure. It also blocks particle leakage, avoids fluid entrainment, uniformizes fluid distribution to enhance adsorption efficiency, shares the bed load, protects the bottom main support structure, and ensures the long-term stable operation of the fixed bed.

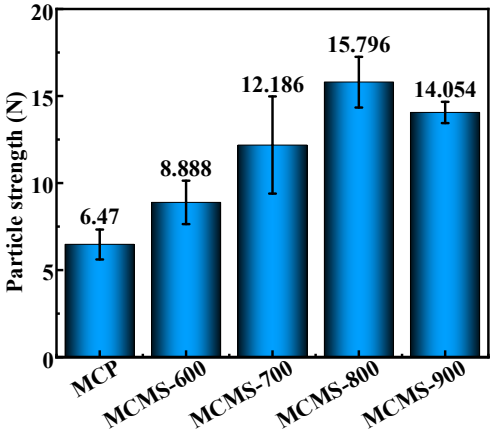

Fig. S5 Mechanical strength of the samples

Section 2 Supporting Tables

Table S1 Relevant physical properties of C4 olefins and paraffin

Table S1 Relevant physical properties of C4 olefins and paraffins.

Hydrocarbon	Boiling point (K)	Kinetic diameter (Å)	Polarizability (Å^3)	Molecular size (Å^3)	Saturated vapor pressure (mPa)
C_4H_6	268.62	4.31	86.4	2.7×4.6×7.3	0.245
n-C_4H_8	266.92	4.46	79.7-85.2	3.5×4.5×7.4	0.247
i-C_4H_8	266.25	4.84	80	3.6×5.2×6.0	0.256
n-C_4H_{10}	272.66	4.69	82.0	3.7×4.0×7.4	0.201
i-C_4H_{10}	261.34	5.28	81.4-82.9	4.5×5.5×6.2	0.288

Table S2 Porosity parameters of the samples

Table S2 The pore structure parameters of MCMSs

Samples	S_{BET} (m^2/g)	V_{total} (cm^3/g)	V_{micro} (cm^3/g)	V_{micro}/V_{total} (%)
MCP	0.3653	0.000330	0.000221	66.96
MCMS-600	229.7044	0.143334	0.084554	58.99
MCMS-700	232.2044	0.142541	0.094730	66.46
MCMS-800	251.1468	0.151045	0.106985	70.83
MCMS-900	280.5940	0.171326	0.117368	68.51

Table S3 Element compositions of the samples from XPS analysis

Table S3 presents the surface chemical compositions of millet and its derived carbon materials (MCMS-X). The data in the table indicate that as the pyrolysis temperature increases, the contents of N and O elements in the resultant samples gradually decrease, which can be attributed to the thermal decomposition of N-containing and O-containing functional groups on the sample surfaces during the pyrolysis process.[5, 6]

Table S3 Element compositions of MCMS-X from XPS

Samples	C/%	(N+O)/%	C/(N+O)
MCP	76.78	21.05	3.75
MCMS-600	87.43	12.57	6.96
MCMS-700	88.29	11.71	7.54
MCMS-800	88.61	11.39	7.78
MCMS-900	90.14	9.86	9.14

Table S4 sp^2-C/sp^3-C ratios of the samples

Table S4 summarizes the sp^2-C/sp^3-C ratios of the millet-derived carbon precursor and MCMS-X series samples, as determined by deconvolution of their C 1s X-ray photoelectron spectroscopy (XPS) spectra. The deconvoluted C 1s spectra consist of three key components: sp^2-hybridized carbon (sp^2-C, corresponding to graphitic carbon), sp^3-hybridized carbon (sp^3-C, corresponding to aliphatic carbon), and carbonyl/quinone groups (C=O).

Table S4 sp^2-C/sp^3-C ratios of the samples

Samples	Relative Concentration (%)			
	sp^2-C	**sp^3-C**	**C=O**	**sp^2-C/sp^3-C**
MCP	62.41	28.66	8.93	2.18
MCMS-600	70.82	21.95	7.23	3.23
MCMS-700	75.08	17.77	7.15	4.23
MCMS-800	79.99	13.52	6.49	5.92
MCMS-900	84.93	10.11	4.96	8.4

Table S5 Comparison of granular MCMS-X and some reported powdery adsorbents

Table S5 Comparison of the as-prepared granular MCMS-X and some reported powdery adsorbents in the aspects of uptakes for C_4H_6, *i*-C_4H_8, and *n*-C_4H_8.

Adsorbents	Temperature (K)	Pressure (bar)	Uptake (mmol/g)			Uptake Ratio		Ref
			C_4H_6	*n*-C_4H_8	*i*-C_4H_8	C_4H_6/*n*-C_4H_8	C_4H_6/*i*-C_4H_8	
MCMS-700	298	1	1.88	0.12	0.008	15.67	235	This Work
MCMS-800	298	1	2.01	0.12	0.04	16.75	50.25	This Work
SC-K	298	1	2.36	0.63	0.50	3.74	4.7	[7]
TMA-VT-5	298	1	0.8	0.7	-	1.14	-	[8]
GeFSIX-14-Cu-i	298	1	2.67	0.57	0.42	4.68	6.4	[9]
NbFSIX-2-Cu-i	298	1	2.64	2.26	0.48	1.17	5.7	[9]
TMOF-1	298	1	1.64	1.08	0.20	1.52	8.2	[10]
ZU-619	298	1	1.58	0.63	0.34	2.51	4.7	[10]
SOFOUR-DPDS-Ni	298	1	1.70	1.42	0.18	1.2	9.4	[11]
Ni-gallate	298	1	1.39	0.57	0.09	2.44	15.4	[12]
ZU-609	298	1	2.19	1.10	0.21	1.99	10.4	[13]
ZU-96	298	1	4.11	2.46	0.22	1.67	11.2	[14]
SIFSIX-Cu-TPB	298	1	3.23	2.73	2.43	1.18	1.3	[15]
TIFSIX-Cu-TPB	298	1	3.35	2.96	2.56	1.13	1.3	[15]
WCMS-500	298	1	1.81	0.52	0.16	3.48	11.3	[16]
WCMS-600	298	1	1.84	0.41	0.22	4.48	8.36	[16]
γ-CD-COF	298	1	2.4	2.2	1.92	1.09	1.25	[17]

References

1. C. Y. Lee, Y.-S. Bae, N. C. Jeong, O. K. Farha, A. A. Sarjeant, C. L. Stern, P. Nickias, R. Q. Snurr, J. T. Hupp and S. T. Nguyen, *Journal of the American Chemical Society*, 2011, **133**, 5228-5231.
2. L. Yang, Y. Liu, F. Zheng, F. Shen, B. Liu, R. Krishna, Z. Zhang, Q. Yang, Q. Ren and Z. Bao, *ACS Nano*, 2024, **18**, 3614-3626.
3. X. Huang, F. Chen, H. Sun, L. Yang, Q. Yang, Z. Zhang, Y. Yang, Q. Ren and Z. Bao, *Journal of the American Chemical Society*, 2024, **146**, 617-626.
4. Z. Bao, S. Alnemrat, L. Yu, I. Vasiliev, Q. Ren, X. Lu and S. Deng, *Journal of Colloid and Interface Science*, 2011, **357**, 504-509.
5. H. Luo, D. Zhou, F. Teng, J. Wang, Q. Xia, X. Zhou and Z. Li, *Science China Materials*, 2025, **68**, 2449-2458.
6. D. Zhou, H. Luo, Y. Yu, X. Zhou, Q. Xia, Y. Wu and Z. Li, *Journal of Materials Chemistry A*, 2025, **13**, 10135-10146.
7. S. Du, X. Wang, J. Huang, K. Kent, B. Huang, I. Karam, Z. Li and J. Xiao, *AIChE Journal*, 2021, **67**, e17285.
8. P. Hu, S. Yao, D. Li, G. Zheng, D. He, Q. Zhu, Y. Li, W. Ueda and Z. Zhang, *Chemical Engineering Journal*, 2023, **452**, 139315.
9. Z. Zhang, Q. Yang, X. Cui, L. Yang, Z. Bao, Q. Ren and H. Xing, *Angewandte Chemie International Edition*, 2017, **56**, 16282-16287.
10. J. Cui, Z. Zhang, J. Hu, L. Yang, Y. Li, L. Chen, X. Cui and H. Xing, *Chemical Engineering Journal*, 2021, **425**, 130580.
11. J. Liu, H. Xiong, H. Shuai, X. Liu, Y. Peng, L. Wang, P. Wang, Z. Zhao, Z. Deng, Z. Zhou, J. Chen, S. Chen, Z. Zeng, S. Deng and J. Wang, *Nature Communications*, 2024, **15**, 2222.
12. J. Chen, J. Wang, L. Guo, L. Li, Q. Yang, Z. Zhang, Y. Yang, Z. Bao and Q. Ren, *ACS Applied Materials & Interfaces*, 2020, **12**, 9609-9616.
13. J. Cui, Z. Qiu, Z. Yang, A. Jin, X. Cui, L. Yang and H. Xing, *Angewandte Chemie International Edition*, 2024, **63**, e202403345.
14. B. Gao, Z. Zhang, J. Hu, J. Cui, L. Chen, X. Cui and H. Xing, *Chinese Journal of Chemical Engineering*, 2022, **42**, 49-54.
15. Y. Liu, Y. Zhang, P. Zhang, Y. Peng, X. Liu, J. Chen, S. Chen, Z. Zeng, J. Wang and S. Deng, *Chemical Engineering and Processing - Process Intensification*, 2022, **172**.
16. R. Wan, H. Luo, X. Sun, Q. Xia, J. Liu, M. Sun, Z. Li and X. Zhou, *Separation and Purification Technology*, 2026, **382**, 135899.
17. X. Chen, in *Proceedings of the 2024 6th International Conference on Civil Engineering, Environment Resources and Energy Materials (CCESEM 2024)*, 2024, DOI: 10.2991/978-94-6463-606-2_44, ch. Chapter 44, pp. 432-438.